Available online at www.sciencedirect.com
ScienceDirect
Trans. Nonferrous Met. Soc. China 35(2025) 474−485

Transactions of
Nonferrous Metals
Society of China
www.tnmsc.cn

Effect of rhenium addition on microstructure and mechanical properties of Ti−48Al−2Cr−2Nb alloys

Sheng-hang XU[1,2,3], Jun-jie LAN[1], Meng HAN[3], Hui-bin ZHANG[1],
Kai-jie SHEN[1], Jun-pin LIN[4], Hua-zhen CAO[1], Guo-qu ZHENG[1]

1. College of Materials Science and Engineering, Zhejiang University of Technology, Hangzhou 310014, China;
2. State Key Laboratory of Powder Metallurgy, Central South University, Changsha 410083, China;
3. Advanced Materials Additive Manufacturing Innovation Research Center, Hangzhou City University, Hangzhou 310015, China;
4. State Key Laboratory for Advanced Metals and Materials, University of Science and Technology Beijing, Beijing 100083, China

Received 14 August 2023; accepted 28 April 2024

Abstract: The refractory metal rhenium (Re), with content of 0−2 at.%, was introduced into a typical γ-TiAl alloy of Ti−48Al−2Cr−2Nb (at.%) through vacuum arc melting. The effect of Re content on the microstructure and mechanical properties of the γ-TiAl alloy was investigated. The results show that the γ-TiAl−xRe alloy is composed of γ, α_2, and β phases. As the Re content increases, the proportion of β phase increases, while the content and size of $\alpha_2+\gamma$ lamellar structure decrease gradually. Furthermore, the compressive strength increases with increasing Re content. A maximum compressive strength of 2282 MPa is achieved for the γ-TiAl−2Re alloy. The γ-TiAl−2Re alloy exhibits a fracture strain of 36.7%, considerably higher than that of the γ-TiAl alloy (31.0%). Moreover, compared with the γ-TiAl alloy, the hardness and compressive strength of the γ-TiAl−2Re alloy considerably increase by 17.5% and 34.2%, respectively.

Key words: γ-TiAl alloy; rhenium; vacuum arc melting; lamellar cluster; mechanical properties; strengthening mechanism

---

1 Introduction

γ-TiAl alloys have the merits of low density, high melting point, and excellent creep resistance and antioxidation performance. Thus, they have been considered a viable alternative to the heavy Ni-based superalloys in the high-temperature applications such as turbine blades in aerospace and power plants [1−3]. Despite the high suitability of γ-TiAl alloys for next-generation aerospace and automotive applications, they were commercially introduced into turbofan engines by GE only after Ti−48Al−2Cr−2Nb (Ti-4822 alloy) blades obtained certification in 2010 [4−6]. In general, the castings of γ-TiAl alloys, particularly Ti-4822 alloy, pose severe processing challenges primarily due to the inherently low ductility associated with their intermetallic phases [7−10]. Limited slip systems in γ-TiAl alloys can also decrease their fracture toughness [11−13]. To overcome these limitations, advanced γ-TiAl alloys with improved mechanical properties and overall performance are being developed by incorporating β-stabilizing elements such as Nb, Ta, W and Cr [14−18]. However, the room-temperature strength and plasticity of γ-TiAl

---

Corresponding author: Hui-bin ZHANG, Tel: +86-571-88320429, E-mail: zhanghb@zjut.edu.cn;
Guo-qu ZHENG, Tel: +86-571-88320429, E-mail: zhenggq@zjut.edu.cn

DOI: https://doi.org/10.1016/S1003-6326(24)66693-8

alloys are still insufficient, limiting their widespread application.

Rhenium (Re), renowned for its exceptionally high melting point of up to 3180 °C, is widely used in nickel-based superalloys to increase their service temperature and high-temperature strength [19−21]. In recent generations of nickel-based superalloys, Re is an essential element, and its usage has been gradually increasing. The introduction of Re can considerably enhance the high-temperature performance of nickel-based superalloys [22−25]. The primary reason for such an enhancement is that Re is mainly concentrated within the γ matrix phase. Re takes part in the formation of atomic clusters with short-range ordered structures, effectively impeding the motion of dislocations. In turn, element diffusion and directional growth rate of γ' phase decrease, thereby improving the mechanical properties and high-temperature performance of superalloys.

The performance of NiAl alloys can be enhanced by adding Re. These alloys have garnered attention as a potential alternative to nickel-based superalloys. BOCHENEK et al [26] studied the impact of Re on the microstructure and the properties of NiAl alloys and reported that Re precipitated at the grain boundaries of NiAl. Additionally, a portion of Re diffused into the NiAl matrix, forming a Re-containing NiAl solid solution. The presence of Re precipitates and its diffusion into the NiAl matrix improved the fracture toughness of NiAl alloys.

The effect of Re on Ti alloys has also been reported. LI et al [27] added Re in the Ti−10Al−4Ta−2Nb−0.25Re alloy, which led to a notable refinement of the secondary α phase. Moreover, the density of the β/α interface increased, thereby impeding dislocation movement and enhancing the strength. MAJCHROWICZ et al [28] added Re in Ti alloys and obtained a highly refined acicular α' martensite structure. Compared with commercial pure Ti, the fine α' needles in the Ti−Re alloy effectively hindered the motion of dislocations, thereby improving its strength. CHLEBUS et al [29] demonstrated that the inclusion of a small amount of dissolved Re in the martensitic structure notably increased the hardness of Ti. When the Re content reached 1.5 at.%, the hardness increased by 85%.

Indeed, the addition of Re into γ-TiAl alloys can result in effective microstructure refinement owing to its high melting point, high activation energy for vacancy conversion, and significant deviation from the lattice size of the γ-TiAl matrix. When Re is dissolved in γ-TiAl alloys, the high activation energy associated with vacancy conversion can effectively hinder the migration of vacancies along the grain boundaries. Additionally, the solid soluble Re can induce substantial lattice distortion, thereby increasing the activation energy for grain boundary migration and inhibiting grain growth during alloy synthesis. Moreover, the substantial difference in atomic radii among Re, Ti and Al can potentially cause solution strengthening, enhancing the mechanical properties of the alloy. Despite the significant potential of Re in enhancing the properties of γ-TiAl alloys, the marked difference in melting points between Re and γ-TiAl alloys has hindered relevant research efforts.

Herein, four Ti−48Al−2Cr−2Nb−xRe (γ-TiAl−xRe, x=0, 0.25, 1, and 2 at.%) alloys with varying Re contents were synthesized via vacuum arc melting. Then, the impact of Re content on the microstructure and mechanical properties of γ-TiAl−xRe alloys was comprehensively investigated. The study is expected to promote the practical application of the rare and precious metal Re in lightweight high-temperature alloys, like γ-TiAl alloys which possess significant engineering implications.

2 Experimental

2.1 Material preparation

γ-TiAl alloys with varying Re contents, Ti−48Al−2Cr−2Nb−xRe (γ-TiAl−xRe, x=0, 0.25, 1, and 2 at.%), were fabricated via vacuum arc melting. The button ingots weighing 100 g, with ~60 mm in diameter and 20 mm in height, were remelted eight times in a water-cooled copper crucible to achieve a homogeneous composition distribution.

2.2 Characterization

Phase identification of bulk samples was performed using a D/max-2550VB X-ray diffraction (XRD) analyzer at room temperature using Cu K_α radiation, operated at 45 kV and 40 mA with a step size of 0.02°. For microstructure observation, the metallographic sample was initially ground using sandpaper to remove surface irregularities. Then, a physical polishing process was used to achieve a smooth and uniform surface. The polished samples were etched using Kroll’s reagent, a mixture of HF, HNO_3, and water with a volume ratio of 5:10:85. After etching, the sample was thoroughly rinsed with alcohol to remove any residual etching solution and then dried under hot air. The etched samples were fist observed using the Olympus-PMG3 optical microscopy (OM). The elemental composition of alloys was determined via scanning electron microscopy (SEM) analysis performed using the Regulus 8100 cold field emission scanning electron microscope equipped with an energy dispersive X-ray spectroscopy (EDS) system operated at an accelerated voltage of 15 kV. An electron back scatter diffraction (EBSD) system (Oxford Instrument), with a step size of 0.5 μm, was used to investigate the elemental distribution, phase maps, and texture. The mechanically polished samples were further electropolished using the Struers TenuPol-5 twin-jet electropolisher in a solution containing 85 vol.% CH_3OH and 15 vol.% HNO_3 at 14 V and −38 °C. Transmission electron microscopy (TEM) was performed on the electropolished samples using the JEM−2100F transmission electron microscope equipped with an EDS system at an accelerating voltage of 200 kV.

The sample for the hardness test was obtained using an electrospark wire electrode cutting technique. The sample underwent grinding and physical post-polishing processes to achieve a smooth surface. Then, its Vickers hardness was measured using the Vickers hardness tester employing a diamond indenter with a load of 9.807 N and a dwell time of 20 s. The average was taken from five hardness test results for each sample and used for analysis.

Room-temperature compression tests were performed on the 858 Mini Bionix II machine with a strain rate of 0.001 s^{-1} using cylindrical specimens with dimensions of d6 mm × 9 mm machined from the ingot along its axis. To ensure the accuracy of results, at least three samples were tested for each condition.

3 Results and discussion

3.1 Phase analysis

Figure 1 shows the XRD patterns of TiAl−xRe alloys. The γ-TiAl and γ-TiAl−0.25Re alloys have diffraction peaks corresponding to the γ-TiAl and α_2-Ti_3Al phases. However, the intensity of α_2-Ti_3Al phase diffraction peak is relatively low. Notably, β phase is not detected when the Re content is <1 at.%, suggesting lower β phase content in these alloys. When the Re content reaches 1 at.%, a diffraction peak corresponding to the β phase was observed. As the Re content increases, the intensity of the β phase diffraction peak increases. Moreover, the diffraction peak of α_2-Ti_3Al phase was nearly absent in the γ-TiAl−2Re alloy.

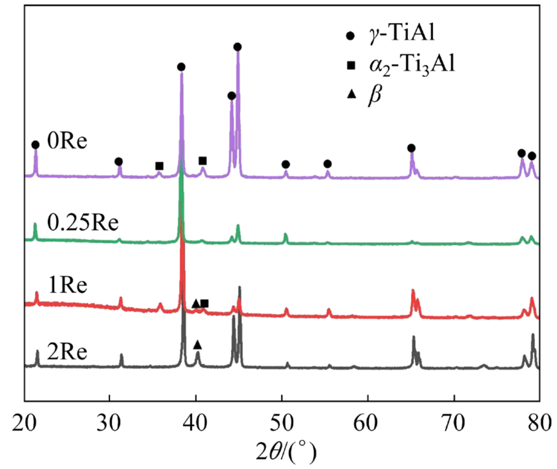

Fig. 1 XRD patterns of γ-TiAl−xRe alloys

3.2 Microstructures of γ-TiAl−xRe alloys

Figure 2 shows the metallographic structure of γ-TiAl−xRe alloys, which reveals their lamellar structure. The γ-TiAl alloy without Re has the largest lamellar clusters (Fig. 2(a)), with an average colony size of ~223.9 μm. Furthermore, fine γ equiaxed crystals near the grain boundary are noticeably visible. As shown in Fig. 2(b), the lamellae of the γ-TiAl−0.25Re alloy are smaller compared to the γ-TiAl alloy, with an average colony size of ~114.7 μm. This suggests that the addition of Re refines the lamellar structure. As the Re content reaches 1 at.%, a higher content of intermittent black mesh can be observed, primarily concentrated at the grain boundaries between lamellae and within the lamellar structure (Fig. 2(c)). Combined with the XRD results, it can be inferred that the black mesh is the β phase. The size of the lamellar colony also decreases significantly (~50.1 μm). As shown in Fig. 2(d), when the Re content reaches 2 at.%, the β phase becomes continuous. Simultaneously, both the size and volume fraction of the lamellar structure considerably decrease.

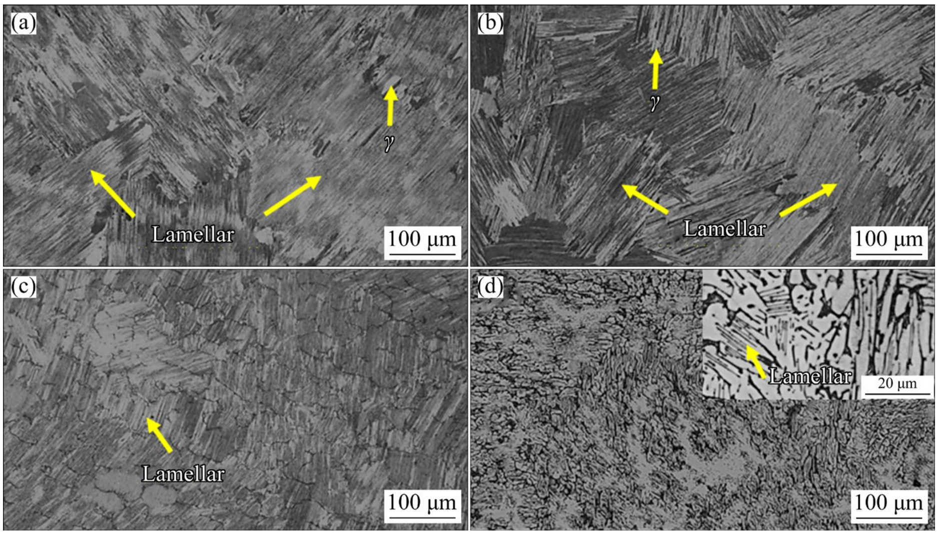

Fig. 2 Metallographic structure of γ-TiAl−xRe alloys: (a) 0Re; (b) 0.25Re; (c) 1Re; (d) 2Re

Figure 3 shows the backscattered electron (BSE) images of γ-TiAl−xRe alloys, which reveal the presence of γ, β, and α_2 phases. Figure 3(a) shows that the γ-TiAl alloy exhibits a typical lamellar structure, which is consistent with the metallographic observation. Combined with the XRD results, it can be concluded that the microstructure of this layer comprises α_2 and γ phases. In contrast, the white areas correspond to the β phase. Thus, the addition of Re considerably modifies the microstructure, as evidenced by grain boundary coarsening and a continuous increase in the β phase content in the alloy. When the Re content is 1 at.%, the majority of β phase is distributed along the grain boundaries, whereas a smaller portion is distributed within the lamellar structure. As the Re content increases to 2 at.%, the β phase content further increases and the volume fraction of the lamellar structure decreases. As a typical β phase–stabilizing element, the incorporation of Re enhances the formation of β phase while inhibits the growth of the lamellar structure.

The chemical composition of γ-TiAl−xRe alloys, corresponding to the marked regions in Fig. 3, is shown in Table 1. In the γ-TiAl alloy, the β phase comprises 5.45 at.% Cr and 2.52 at.% Nb. In the γ-TiAl−1Re alloy, the β phase is composed of 5.66 at.% Cr, 2.52 at.% Nb, and 3.02 at.% Re. As the Re content increases to 2 at.%, the β phase contains 5.74 at.% Cr, 2.10 at.% Nb, and 5.12 at.% Re. Additionally, the Re content in the γ and α_2+γ phases is relatively low.

The EBSD results of the microstructure of γ-TiAl−0.25Re alloy are shown in Fig. 4 with a phase map (Fig. 4(a)) and boundary angle map (Fig. 4(b)). As can be seen from Fig. 4(a), the γ-TiAl−0.25Re alloy is mainly composed of a large columnar α phase due to the formation of coarse columnar crystals induced by the temperature gradient during cooling. Furthermore, considerably smaller and fewer γ/α_2 and β particles are aggregated beside the columnar α phase. Figure 4(c) shows the grain size distribution, which indicates that the average grain size is 116.3 μm, close to that obtained from the OM image (114.7 μm). Figure 4(d) shows the misorientation angle of the adjacent phase. Almost all the high angle boundaries are about 60°, indicating a high density of twin intersections in the γ phase.

Figure 5 shows the pole figures of the γ phase in the γ-TiAl−0.25Re alloy, which exhibits a strong texture of over 6 times random in its (100) direction. Such a robust texture indicates that the cooling rate is below the critical level required for extensive transformation. Specifically, the γ phase precipitates from the α phase with twelve distinct orientation variants, resulting in a more randomized orientation of lamellae.

Figure 6 shows the bright field images of γ-TiAl and γ-TiAl−2Re alloys, revealing their characteristic laminated structures. This laminated structure is composed of α_2 and γ phases, as inferred from the SAED patterns in the inset image. Table 2 shows the cluster size and thickness of the γ and α_2 phases in γ-TiAl alloys with different Re contents.

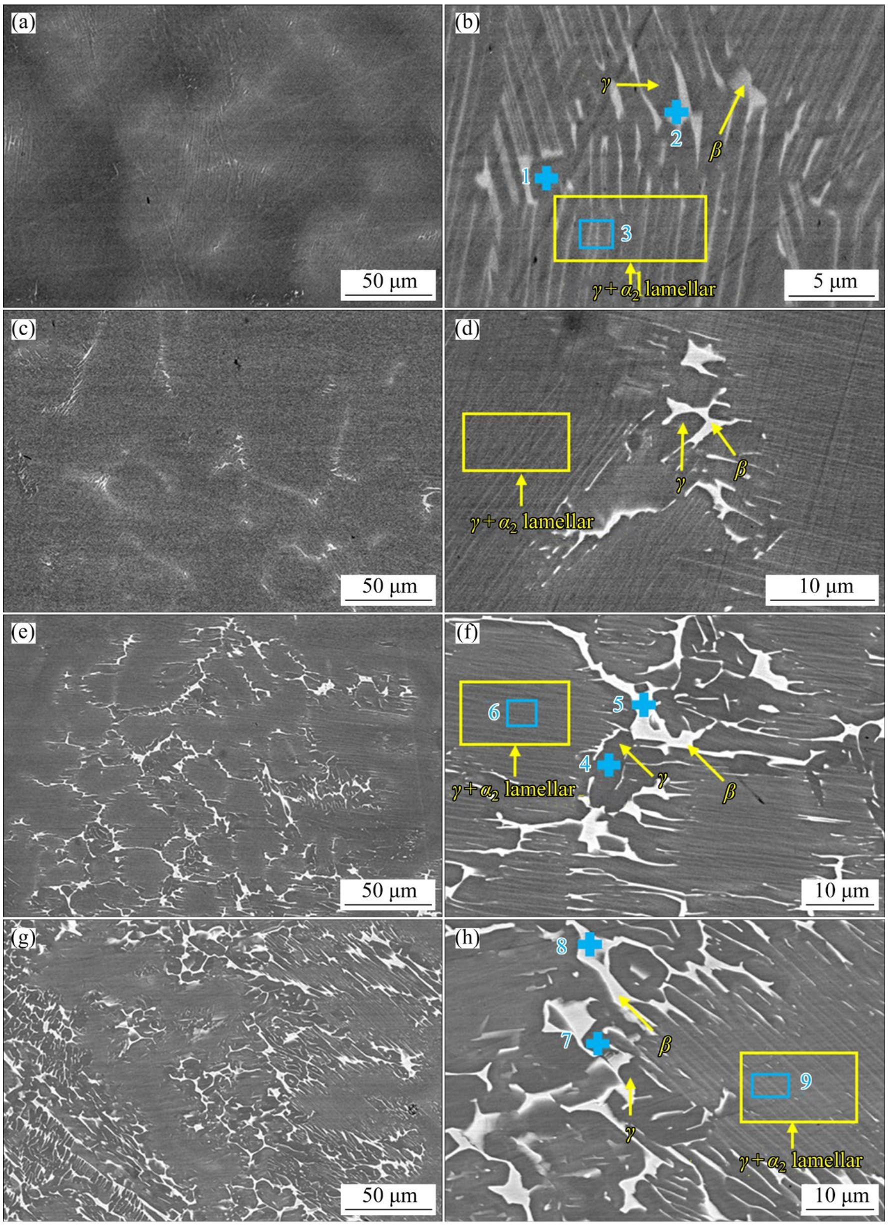

Fig. 3 BSE images of γ-TiAl−*x*Re alloys: (a, b) 0Re; (c, d) 0.25Re; (e, f) 1Re; (g, h) 2Re

Table 1 Chemical composition of γ-TiAl−*x*Re alloys marked regions in Fig. 3

Region	Content/at.%					Phase
	Ti	Al	Cr	Nb	Re	
1	49.47	46.31	1.77	2.45		γ
2	52.53	39.51	5.45	2.52		β
3	50.38	45.27	2.00	2.35		$\alpha_2+\gamma$
4	47.32	48.34	1.37	2.23	0.73	γ
5	54.11	34.69	5.66	2.52	3.02	β
6	48.72	46.80	1.47	2.22	0.79	$\alpha_2+\gamma$
7	49.29	46.26	1.34	2.11	1.01	γ
8	52.88	34.15	5.74	2.10	5.12	β
9	49.64	45.09	1.81	1.95	1.51	$\alpha_2+\gamma$

Specifically, the average thicknesses of the γ and α_2 phases in γ-TiAl alloys are approximately 0.49 and 0.29 μm, respectively. In contrast, the average thicknesses of the γ and α_2 phases in the γ-TiAl−2Re alloy are 0.38 and 0.052 μm, respectively. Evidently, the addition of Re does not have a considerable impact on the γ-phase thickness, but the thickness of the α_2 phase noticeably reduces.

TEM−EDS elemental mapping was performed to further investigate the distribution of Re in the γ-TiAl−2Re alloy (Fig. 7). Results show that both α_2 and γ phases contain small amounts of Re, whereas the β phase contains high content of Re.

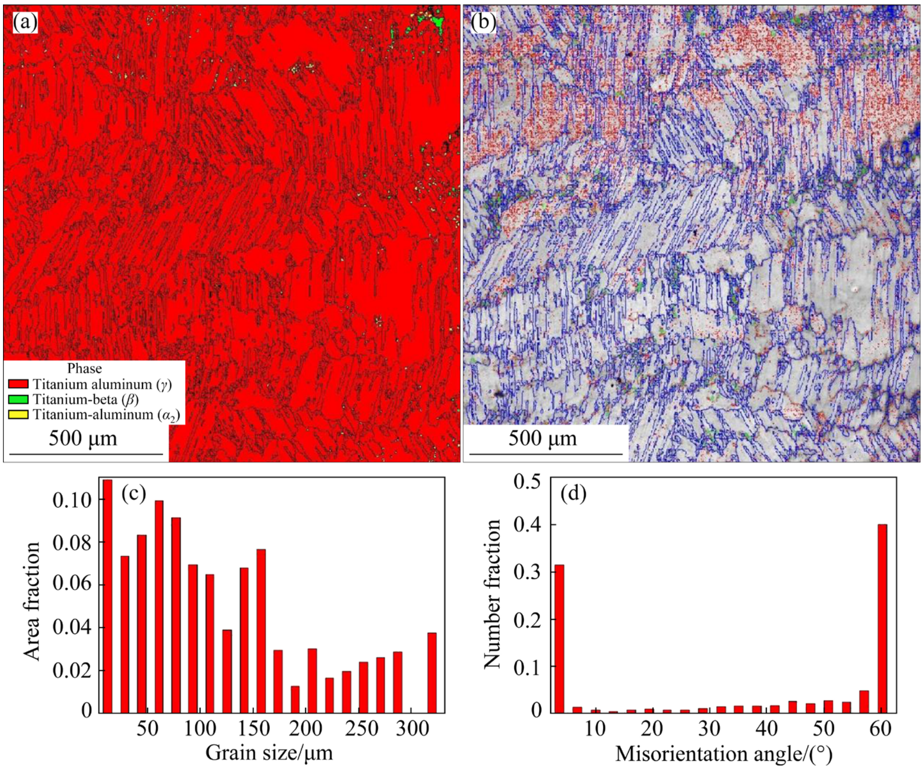

Fig. 4 EBSD analysis of γ-TiAl−0.25Re alloy: (a) Phase map of γ, β, and α_2; (b) Boundary angle; (c) Distribution of grain size; (d) Misorientation angle

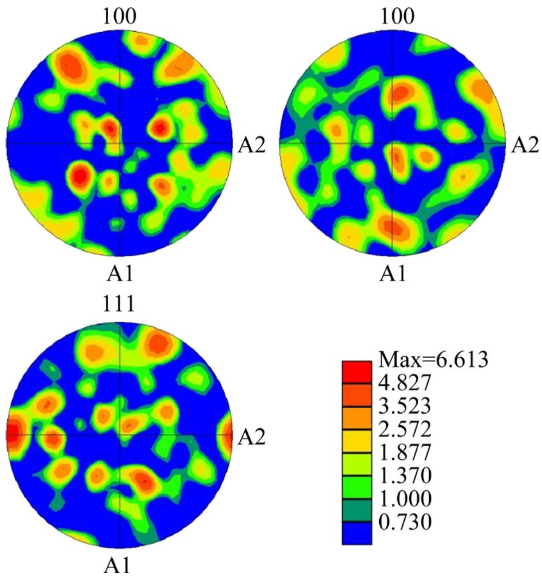

Fig. 5 Pole figures of γ phase in γ-TiAl−0.25Re alloy

This suggests that increasing the Re content promotes the transformation of the α_2 phase into β phase. The transformation is further supported by the XRD patterns, which confirm the absence of α_2 phase in the γ-TiAl−2Re alloy. As the Re content increases, the number of $\gamma+\alpha_2$ layers decreases while that of γ+β structures increases in the γ-TiAl−2Re alloy. This finding is consistent with the results reported by IMAEV et al [30]. Combined with SEM results, the growth of the β(*B*2) phase is deemed mainly due to the $\alpha_2 \rightarrow \beta(B2)$ phase transition, which can be explained by the instability of α_2 phase oversaturated by Mo and Nb.

Table 2 Colony size and thickness of γ and α_2 phases in γ-TiAl−*x*Re alloys

Alloy	Size of lamellar colony/μm	Thickness of γ phase/μm	Thickness of α_2 phase/μm
γ-TiAl	223.9	0.49	0.29
γ-TiAl−0.25Re	114.7	0.46	0.13
γ-TiAl−1Re	50.1	0.41	0.079
γ-TiAl−2Re	20.0	0.38	0.052

TEM results confirm the prevalence of Re in the β phase of TiAl alloys. However, the precise identification of the specific location of Re within the TiAl lattice remains a formidable task. The occupancy and mode of occupancy of Re in the TiAl lattice have been extensively studied using first-principles methods. JIANG [31] used first-principles calculations to investigate the spatial

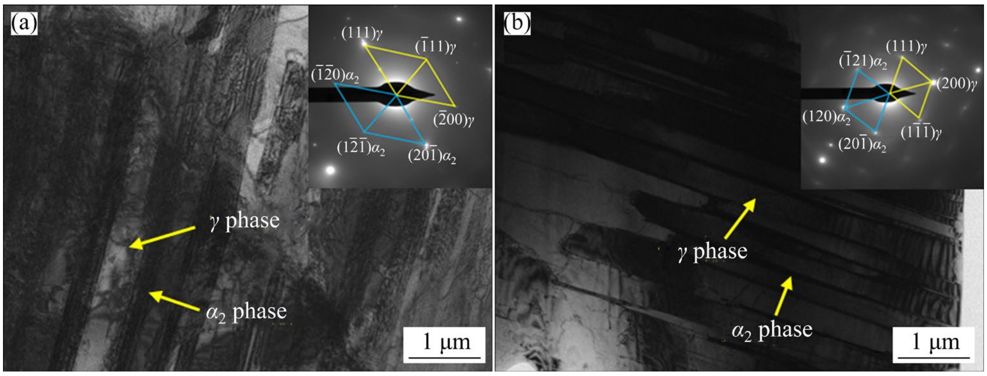

Fig. 6 TEM images of TiAl−*x*Re alloys with SAED images in inset: (a) 0Re; (b) 2Re

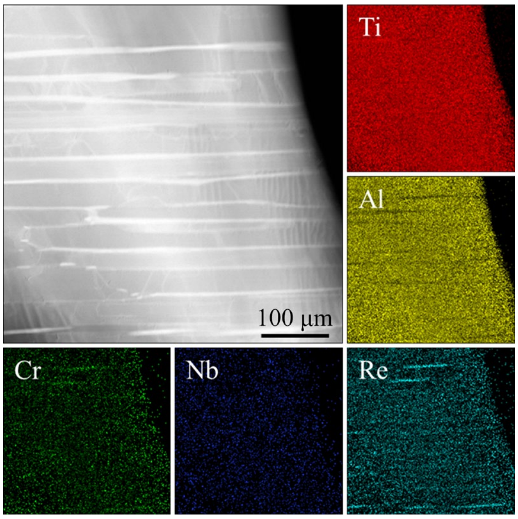

Fig. 7 EDS elemental mappings of γ-TiAl−2Re alloys

occupancy of 3d, 4d, and 5d transition metal solutes in a TiAl alloy with an $L1_0$ structure and revealed that Re exhibited a notable preference for occupying Al sites. OUADAH et al [32] calculated the formation energy of substitute elements in both Ti_3Al and TiAl phases and suggested that Re was more prone to dissolve into the α_2-Ti_3Al phase. Furthermore, the increase in Re content predominantly contributed to the transformation of the α_2 phase into β phase, thereby explaining the observed increase in the proportion of β phase.

3.3 Mechanical properties

3.3.1 Vickers hardness

Table 3 shows the Vickers hardness of the γ-TiAl−*x*Re alloys. As the Re content increases from 0 to 0.25 at.%, the hardness of the γ-TiAl alloy increases rapidly and considerably from HV 275.0 to HV 359.4 because the grain size decreases with increasing Re content. According to the Hall−Petch formula, the strength is inversely proportional to the square root of the grain size, and a higher strength implies higher hardness [33,34]. The β phase content increases with increasing addition of Re in the γ-TiAl alloy. β phase displays the highest hardness among all the phases in the γ-TiAl alloy [35], thereby increasing its hardness. The addition of Re can result in solid solution hardening. The SEM−EDS results suggest that Re has a certain solubility in both γ and α_2 phases, causing solid solution hardening of the γ-TiAl−*x*Re alloy. However, the hardness slightly decreases as the Re content reaches 2 at.%. The XRD results reveal that the α_2 phase content decreases and the γ phase content increases in the γ-TiAl−2Re alloy. The α_2 phase has higher hardness than the γ phase, which reduces the overall hardness of the alloy. XU et al [36] studied the effect of Mo content on the microstructure and mechanical properties of the γ-TiAl alloy. The results showed that as the Mo content increased, the volume fraction of α_2 phase decreased rapidly whereas that of γ phase increased considerably, thereby decreasing the hardness. Moreover, the combined SEM and OM results show that the lamellar structure in the alloy decreases as the Re content increases. This phenomenon enhances the hardness, as the γ/α_2 interface in the structure effectively inhibits dislocation movement. Hence, the hardness of the γ-TiAl−2Re alloy is reduced.

Table 3 Vickers hardness of γ-TiAl−*x*Re alloys

Re content/ at.%	Vickers hardness (HV)					Average hardness (HV)
0	280	268	266	290	271	275.0
0.25	363	354	362	352	366	359.4
1	349	352	339	365	351	351.2
2	320	322	315	328	331	323.2

3.3.2 Compression properties and fracture morphologies

Figure 8(a) shows the compressive stress–strain curves of γ-TiAl−xRe alloys with varying Re content. The plastic deformation stage of the alloys exceeds the elastic deformation stage during compression at room temperature. This implies that these alloys possess a remarkable ability to undergo plastic deformation and exhibit significant work hardening capacity under uniaxial compressive stress. The compressive strength of γ-TiAl−xRe alloys is considerably higher than that without Re. In the γ-TiAl alloy, the compressive strength is 1700 MPa with a fracture strain of 31.0%. The compressive strength of the alloy increases considerably to 1879 MPa (a 10.52% increase) when the Re content is increased to 0.25 at.%. However, the fracture strain remains almost unchanged. Further increasing the Re content to 1 at.% increases the compressive strength of the alloy to 2021 MPa, 18.88% increase compared with the γ-TiAl alloy. The fracture strain of γ-TiAl−xRe sample also increases from 31.0% to 37.8%. When the Re content in the γ-TiAl alloy reaches 2 at.%, its compressive strength further increases to 2282 MPa, with a fracture strain of 36.7%. The compressive strength increases by 34.23% compared with the γ-TiAl alloy. Figure 8(b) shows the variation in the yield strength for the γ-TiAl alloys with different Re contents. As the Re content increases up to 1 at.%, the yield strength of the alloy increases from (393±26) to (803±32) MPa. However, when the Re content surpasses 1 at.%, the yield strength begins to decrease, reaching (604±28) MPa at 2 at.%.

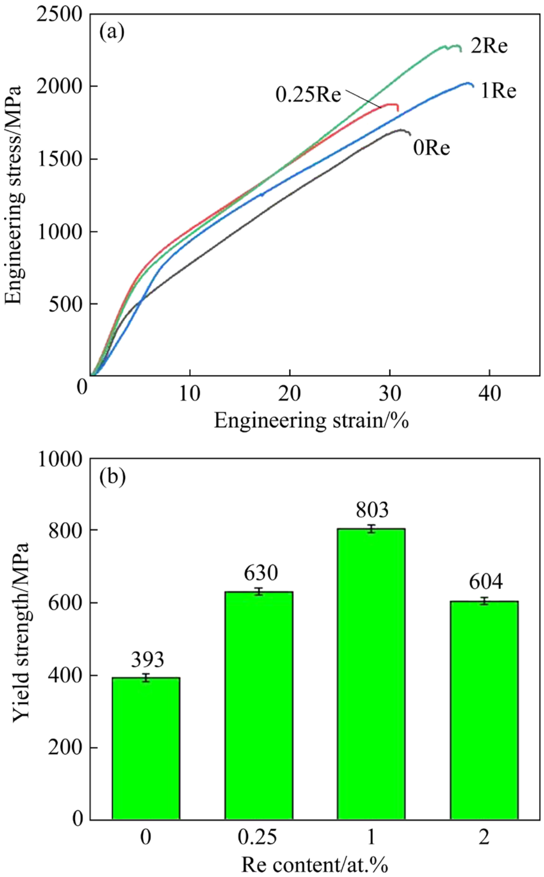

Fig. 8 Compressive stress–strain curves (a) and yield strength (b) of γ-TiAl−xRe alloys

The compressive strength of the γ-TiAl alloy increases with increasing Re content because of the following reasons. (1) The elemental mappings in Fig. 8 show that Re is soluble in the matrix, indicating the solid solution strengthening effect. As Re atom is relatively large, its integration into the Al lattice causes distortion and subsequent alloy strengthening. (2) The SEM and OM images reveal that the addition of Re leads to an increase of the β phase. The β phase in the γ-TiAl usually precipitates along the grain boundaries, hindering the grain growth and refining the grain boundary. According to the Hall−Petch formula, $\sigma_s=\sigma_0+kd^{-1/2}$, a smaller grain size results in an increase in its yield strength. Furthermore, the increasing Re content can also refine the γ/α_2 layer structures, considerably hindering the slip of dislocations. As shown in Table 2, the thicknesses of γ and α_2 phases within the γ-TiAl−1Re alloy decrease to 0.41 and 0.079 μm, respectively, lower than those of the γ-TiAl alloy (0.49 and 0.29 μm, respectively). As the Re content increases to >1 at.%, the yield strength of the alloy decreases. As Re is a β phase–stabilizing element, higher Re contents can impede the phase transformation of β to α and subsequently to α_2. The α_2 phase inhibits crack propagation at the intersection points by causing kinks and necking [37]. As the α_2 phase content decreases, its corresponding inhibitions reduce and the yield strength decreases. The microstructure of alloys also decreases the yield strength. In particular, the volume fraction of the lamellar structure decreases as the Re content increases, which plays a crucial role in impeding the slip of dislocations and increasing the yield strength.

When the Re content in the alloy is 1 and 2 at.%, the fracture strain increases considerably because the addition of Re induces significant grain refinement, which enhances the coordination of plastic deformation within the alloy. Meanwhile, the reduction of the crystal axis ratio *c*/*a* would be another reason. CHUBB et al [38] reported that the symmetry of the $L1_0$ structure was enhanced when the *c*/*a* value approached 1, thereby improving the fracture strain of the alloy. JIANG [31] investigated the impact of alloying elements on the *c*/*a* ratio of the *γ*-TiAl lattice with $L1_0$ structure using first-principles calculations. Their results showed that the introduction of Re considerably reduced the *c*/*a* ratio of the TiAl alloy. The *c*/*a* ratio reached ~1.005 when Re occupied the position of Al. The XRD results show the *c*/*a* values in the *γ*-TiAl, *γ*-TiAl−1Re, and *γ*-TiAl−2Re alloys are 1.0152, 1.0144 and 1.0147, respectively, calculated using the Jade6.0 software (Table 4). This indicates that the addition of Re reduces the c/a value. A smaller c/a value promotes a more uniform distribution of stress and strain in the microstructure, allowing for substantial plastic deformation process before fracture. The p–d bond interaction also decreases. The Al−Ti p–d covalent bond within the alloy has directional properties. The pronounced directionality of the covalent bonds enhanced the shear strength and significantly inhibited shear deformation [39]. Re, a 5d transition metal, has a large number of d-orbital electrons. Introducing Re atoms into the *γ*-TiAl alloy can potentially increase the charge overlap density around the transition metal and nearby Ti atoms, thereby reducing the Ti−Al bond interaction and enhancing the Ti−Ti bond interaction. Consequently, the overall fracture strain of the *γ*-TiAl alloy is improved.

Table 4 Lattice parameters of *γ* phase in *γ*-TiAl−*x*Re alloys

Alloy	*c*/*a*
TiAl−0Re	1.0152
TiAl−1Re	1.0144
TiAl−2Re	1.0147

The majority of the *γ*-TiAl−*x*Re alloys exhibit shear fracture along 45°, relative to the loading direction under compression. Figure 9 shows the

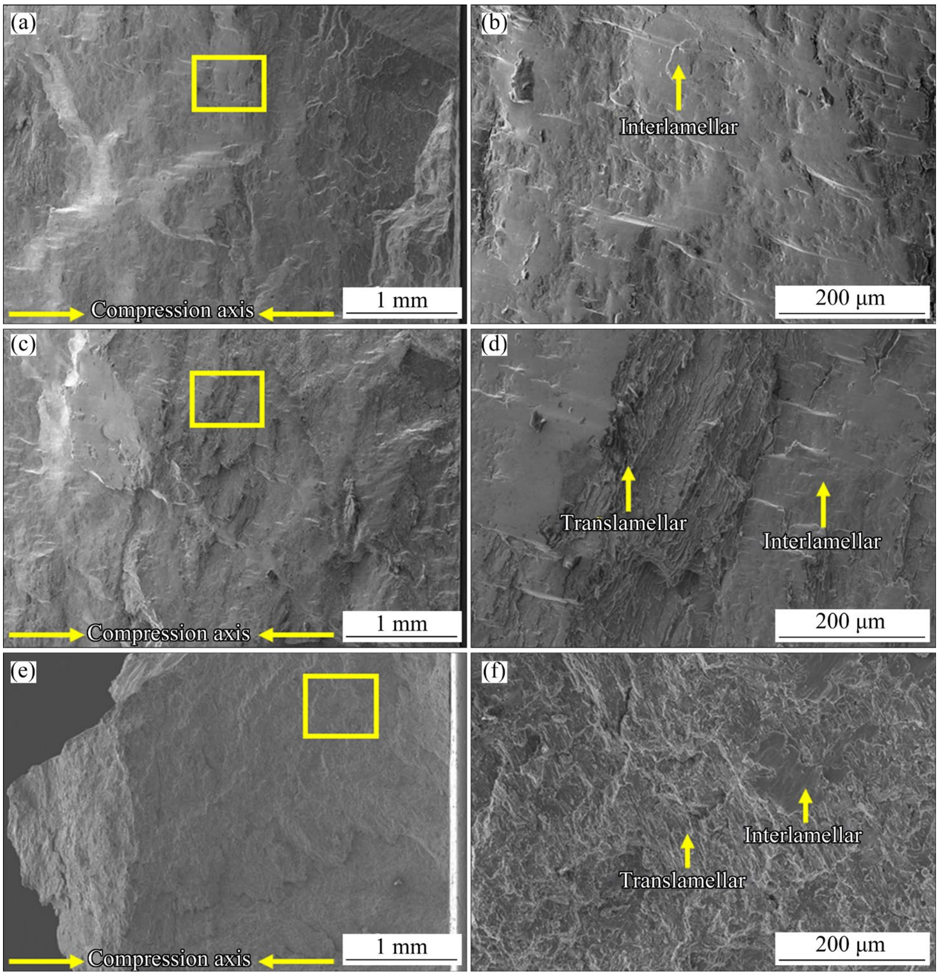

Fig. 9 Fracture morphologies of TiAl−*x*Re alloys: (a, b) 0Re; (c, d) 1Re; (e, f) 2Re

fracture morphology of the γ-TiAl−xRe alloy after compression. Figures 9(a, b) show that the fracture surface of the γ-TiAl alloy has a high proportion of interlaminar cleavage planes and a small proportion of translamellar fracture planes. The fracture surface also shows numerous slip lines, indicating significant deformation before failure. The predominant mode of fracture is interlamellar, which is characterized by cracks initiating and propagating between lamellae. The fracture mode of the γ-TiAl−1Re alloy comprises interlamellar and translamellar fractures, with tiny dimples on the fracture surface (Figs. 9(c, d)). Moreover, the fracture surface of the γ-TiAl−1Re alloy shows more number of translamellar cracks than that of the γ-TiAl alloy. As the Re content reaches 2 at.%, the proportion of cleavage planes decreases considerably, whereas that of tearing edges increases (Figs. 9(e, f)). The fracture surface also shows an increased proportion of dimples, indicating improved plasticity.

4 Conclusions

(1) The microstructure of the γ-TiAl-xRe alloys contains α_2, γ-TiAl, and β phases. As the Re content increases, the grain boundary coarsens and the β phase content increases.

(2) The addition of Re in the γ-TiAl alloy can enhance its strength and hardness via solid solution strengthening and fine-grain strengthening mechanisms.

(3) The fracture strains of the γ-TiAl−1Re and the γ-TiAl−2Re alloys are obviously improved due to the fine-grain strengthening, reaching 37.8% and 36.7%, respectively.

(4) The hardness, compressive strength, and fracture strain of the γ-TiAl−2Re alloy considerably increase to 17.5%, 34.2%, and 18.3%, respectively, compared with those of the γ-TiAl alloy.

CRediT authorship contribution statement

Sheng-hang XU: Methodology, Funding acquisition, Writing − Review & editing; **Jun-jie LAN:** Data curation, Writing − Review & editing; **Meng HAN:** Investigation, Data curation; **Hui-bin ZHANG:** Investigation; **Kai-jie SHEN:** Data curation; **Jun-pin LIN:** Supervision, Funding acquisition; **Hua-zhen CAO:** Resources, Investigation; **Guo-qu ZHENG:** Conceptualization, Project administration, Resources, Supervision.

Declaration of competing interest

The authors declare that they have no known competing financial interests or personal relationships that could have appeared to influence the work reported in this paper.

Acknowledgments

This work was supported by the Natural Science Foundation of Zhejiang Province, China (No. LQ21E040004), the National Natural Science Foundation of China (No. 52271040), the State Key Lab of Advanced Metals and Materials, China (No. 2021-Z03), and the State Key Laboratory of Powder Metallurgy, Central South University, China.

References

[1] WANG Lin, SHEN Chen, ZHANG Yue-long, LI Fang, HUANG Ye, DING Yu-han, XIN Jian-wen, ZHOU Wen-lu, HUA Xue-ming. Effect of Al content on the microstructure and mechanical properties of γ-TiAl alloy fabricated by twin-wire plasma arc additive manufacturing system [J]. Materials Science and Engineering A, 2021, 826: 142008.

[2] YUE Hang-yu, PENG Hui, LI Rui-feng, GAO Run-qi, WANG Xiao-peng, CHEN Yu-yong. High-temperature microstructure stability and fracture toughness of TiAl alloy prepared via electron beam smelting and selective electron beam melting [J]. Intermetallics, 2021, 136: 107259.

[3] GE Geng-wu, WANG Ze-ming, ZHANG Lai-qi, LIN Jun-pin. Hot deformation behavior and artificial neural network modeling of β-γ TiAl alloy containing high content of Nb [J]. Materials Today Communications, 2021, 27: 102405.

[4] XU Run-run, LI Miao-quan, ZHAO Yong-hao. A review of microstructure control and mechanical performance optimization of γ-TiAl alloys [J]. Journal of Alloys and Compounds, 2023, 932: 167611.

[5] TIAN Shi-wei, HE An-rui, LIU Jian-hua, ZHANG Ye-fei, YANG Yong-gang, ZHANG Yun, JIANG Hai-tao. Oxidation resistance of TiAl alloy improved by hot-pack rolling and cyclic heat treatment [J]. Materials Characterization, 2021, 178: 111196.

[6] LIU Shi-qiu, DING Hong-sheng, CHEN Rui-run, GUO Jing-jie, FU Heng-zhi. Remarkable improvement in tensile strength of a polycrystalline γ-TiAl-based intermetallic alloy by deformation nanotwins [J]. Materials Science and Engineering A, 2021, 823: 141692.

[7] GUO Ying-fei, CHEN Yu-yong, XIAO Shu-long, TIAN Jing, ZHENG Zhuang-zhuang, XU Li-juan. Influence of nano-Y_2O_3 addition on microstructure and tensile properties of high-Al TiAl alloys [J]. Materials Science and Engineering A, 2020, 794: 139803.

[8] DUAN Bao-hua, YANG Yu-chen, HE Shi-yu, FENG Qi-sheng, MAO Lu. ZHANG Xue-xian, JIAO Li-na, LU Xiong-gang, CHEN Guang-yao, LI Chong-he. History and development of γ-TiAl alloys and the effect of alloying elements on their phase transformations [J]. Journal of Alloys and Compounds, 2022, 909: 164811.

[9] XU Xue-song, DING Hong-sheng, HUANG Hai-tao, LIANG He, CHEN Rui-run, GUO Jing-jie, FU Heng-zhi. Effect of V on the microstructure and brittle-to-ductile transition of directionally solidified high-Nb TiAl alloy [J]. Intermetallics, 2022, 142: 107455.

[10] GAO Qiang, ZHANG Lai-qi, QIAO Yi, LIN Jun-pin. Diffusion bonding behaviour of β-γ TiAl alloys containing high niobium with Ti interlayer by spark plasma sintering [J]. Transactions of Nonferrous Metals Society of China, 2022, 32: 3973−3984.

[11] LIU Zhang-qi, WANG Chen-yang, WANG Wen-bo, XU Guo-jian, LIU Xiang-yu. Effects of tantalum on the microstructure and properties of Ti−48Al−2Cr−2Nb alloy fabricated via laser additive manufacturing [J]. Materials Characterization, 2021, 179: 111317.

[12] YOUN S J, KIM Y K, KIM H S, LEE K A. Improvement in the high temperature mechanical properties of additively manufactured Ti−48Al−2Cr−2Nb alloy using heat treatment [J]. Intermetallics, 2023, 153: 107784.

[13] GHORBANI H R, KERMANPUR A, REZAEIAN A, SADEGHI F, SIAHBOUMI A A. Solidification behavior and microstructural features of the cast and HIPed N-bearing Ti−48Al−2Cr−2Nb intermetallic alloys [J]. Journal of Materials Research and Technology, 2023, 24: 5215−5234.

[14] SIAHBOUMI A A, KERMANPUR A, GHORBANI H R, BELOVA L. Effect of hafnium addition on microstructure and room temperature mechanical properties of the Ti−48Al−2Cr−2Nb intermetallic alloy [J]. Journal of Alloys and Compounds, 2022, 917: 165467.

[15] IMAYEV R M, IMAYEV V M, OEHRING M, APPEL F. Alloy design concepts for refined gamma titanium aluminide based alloys [J]. Intermetallics, 2007, 15: 451−460.

[16] ISMAEEL A, WANG C S. Effect of Nb additions on microstructure and properties of γ-TiAl based alloys fabricated by selective laser melting [J]. Transactions of Nonferrous Metals Society of China, 2019, 29: 1007−1016.

[17] HU Yuan-tao, ZHENG Lei, YAN Hao-jie. WU Lian-kui, LIN Xiang-jun, CAO Fa-he, JIANG Mei-yan. Improving hot corrosion resistance of aluminized TiAl alloy by anodization and pre-oxidation [J]. Transactions of Nonferrous Metals Society of China, 2021, 31: 193−206.

[18] HAN Jian-chao, DONG Jing, ZHANG Shu-zhi, ZHANG Chang-jiang, XIAO Shu-long, CHEN Yu-yong. Microstructure evolution and tensile properties of conventional cast TiAl-based alloy with trace Ni addition [J]. Materials Science and Engineering A, 2018, 715: 41−48.

[19] LAKSHMI PRASAD B S, PAJA ANNAMALAI A. Effect of rhenium addition on tungsten heavy alloys processed through spark plasma sintering [J]. Ain Shams Engineering Journal, 2021, 12: 2957−2963.

[20] LIU Y D, LI W. Inhibiting effect of Ni/Re diffusion barrier on the interdiffusion between Ni-based coating and titanium alloys [J]. Materials Today Communications, 2023, 35: 106192.

[21] HUANG Ming, ZHU Jing. An overview of rhenium effect in single-crystal superalloys [J]. Rare Metals, 2016, 35: 127−139.

[22] LI Xiao-bing, XU Hao, XING Wei-wei, CHEN Bo, SHU Lei. ZHAN Meng-shu, LIU Kui. Microstructural evolution and mechanical properties of forged β-solidified γ-TiAl alloy by different heat treatments [J]. Transactions of Nonferrous Metals Society of China, 2022, 32: 2229−2242.

[23] TIAN Su-gui, WU Jing, SHU De-long, SU Yong, YU Hui-chen, QIAN Ben-jiang. Influence of element Re on deformation mechanism within γ' phase of single crystal nickel-based superalloys during creep at elevated temperatures [J]. Materials Science and Engineering A, 2014, 616: 260−267.

[24] SHANG Zhao, NIU Hui-jun, WEI Xiao-peng, SONG Da-zhuo, ZOU Jun-tao, LIU Gang, LIANG Shu-hua, NIE Li-ping, GONG Xiu-fang. Microstructure and tensile behavior of nickel-based single crystal superalloys with different Re contents [J]. Journal of Materials Research and Technology, 2022, 18: 2458−2469.

[25] ZHANG Jia-chen, HUANG Tai-wen, LU Fan, CAO Kai-li, WANG Dong, ZHANG Jian, ZHANG Jian, SU Hai-jun, LIU Lin. The effect of rhenium on the microstructure stability and γ/γ' interfacial characteristics of Ni-based single crystal superalloys during long-term aging [J]. Journal of Alloys and Compounds, 2021, 876: 160114.

[26] BOCHENEK K, WĘGLEWSKI W, MORGIEL J, BASISTA M. Influence of rhenium addition on microstructure, mechanical properties and oxidation resistance of NiAl obtained by powder metallurgy [J]. Materials Science and Engineering A, 2018, 735: 121−130.

[27] LI Juan, XU Ya-qun, XIAO Wen-long, MA Chao-li, HUANG Xu. Development of Ti−Al−Ta−Nb−(Re) near-α high temperature titanium alloy: Microstructure, thermal stability and mechanical properties [J]. Journal of Materials Science & Technology, 2022, 109: 1−11.

[28] MAJCHROWICZ K, PAKIEŁA Z, BRYNK T, ROMELCZYK-BAISHYA B, PŁOCINSKA M, KURZYNOWSKI T, CHLEBUS E. Microstructure and mechanical properties of Ti−Re alloys manufactured by selective laser melting [J]. Materials Science and Engineering A, 2019, 765: 138290.

[29] CHLEBUS E, KUŹNICKA B, DZIEDZIC R, KURZYNOWSKI T. Titanium alloyed with rhenium by selective laser melting [J]. Materials Science and Engineering A, 2015, 620: 155−163.

[30] IMAEV V M, IMAEV R M, OLENEVA T I, KHISMATULLIN T G. Microstructure and mechanical properties of the intermetallic alloy Ti−45Al−6(Nb,Mo)−0.2B [J]. Physics of Metals & Metallography, 2008, 106: 641−648.

[31] JIANG Chao. First-principles study of site occupancy of dilute 3 d, 4 d and 5 d transition metal solutes in L10 TiAl [J]. Acta Materialia, 2008, 56: 6224−6231.

[32] OUADAH O, MERAD G, ABDELKADER H.S. Atomistic modelling of the γ-TiAl/α_2−Ti_3Al interfacial properties affected by solutes [J]. Materials Chemistry and Physics, 2021, 257: 123434.

[33] WEI Ye, ZHANG Ying, LU Huang-hong, XU Hui-bin. Effects of transition metals in a binary-phase TiAl−Ti_3Al alloy: From site occupancy, interfacial energetics to mechanical properties [J]. Intermetallics, 2012, 31: 105−113.

[34] FAN Jiang-lei, LIU Jian-xin, TIAN Shu-xia, WU Shen,

WANG Sheng-yong, GAO Hong-xia, GUO Jing-jie, WANG Xiao, SU Yan-qing, FU Heng-zhi. Effect of solidification parameters on microstructural characteristics and mechanical properties of directionally solidified binary TiAl alloy [J]. Journal of Alloys and Compounds, 2015, 650: 8−14.

[35] ZHENG Y, ZHAO L, TANGRI K. Microstructure evolution during heat treatment of a Cr-bearing Ti_3Al+TiAl alloy [J]. Scripta Metallurgica et Materialia, 1992, 26: 219−224.

[36] XU Wen-chen, HUANG Kai, WU Shi-feng, ZONG Ying-ying, SHAN De-bin. Influence of Mo content on microstructure and mechanical properties of β-containing TiAl alloy[J]. Transactions of Nonferrous Metals Society of China, 2017, 27: 820−828.

[37] NONAKA K, TANOSAKI K, FUJITA M, CHIBA A, KAWABATA T, IZUMI O. Deformation and fracture behavior of TiAl in compression tests at room temperature [J]. Materials Transactions, JIM, 1992, 33: 802−810.

[38] CHUBB S R, PAPACONSTANTOPOULOS D A, KLEIN B M. First-principles study of L10 Ti−Al and V−Al alloys [J]. Physical Review B, Condensed Matter, 1988, 38: 12120−12124.

[39] MORINAGA M, SAITO J, YUKAWA N, ADACHI H. Electronic effect on the ductility of alloyed TiAl compound [J]. Acta Metallurgica et Materialia, 1990, 38: 25−29.

铼添加对 Ti−48Al−2Cr−2Nb 合金显微组织和力学性能的影响

徐圣航 1,2,3，兰俊杰 1，韩 梦 3，张惠斌 1，沈凯杰 1，林均品 4，曹华珍 1，郑国渠 1

1. 浙江工业大学 材料科学与工程学院，杭州 310014；
2. 中南大学 粉末冶金国家重点实验室，长沙 410083；
3. 浙大城市学院 先进材料增材制造创新研究中心，杭州 310015；
4. 北京科技大学 新金属材料全国重点实验室，北京 100083

摘 要：通过真空电弧熔炼方法在 Ti−48Al−2Cr−2Nb 合金中加入含量为 0−2%(摩尔分数)的难熔金属铼(Re)，研究 Re 含量对 γ-TiAl−xRe 合金显微组织和力学性能的影响规律。结果表明：γ-TiAl−xRe 合金由 γ、α_2 和 β 相组成，且随着 Re 含量的增加，β 相的比例增加，$\alpha_2+\gamma$ 片层结构的含量和尺寸逐渐减小。γ-TiAl 合金的抗压强度随 Re 含量的增加而提高，γ-TiAl−2Re 合金的抗压强度最高，达到 2282 MPa。同时，γ-TiAl−2Re 合金的断裂应变为 36.7%，明显高于 γ-TiAl 合金的断裂应变(31.0%)。此外，与 γ-TiAl 合金相比，γ-TiAl−2Re 合金的硬度和抗压强度分别提高了 17.5%和 34.2%。

关键词：γ-TiAl 合金；铼；真空电弧熔炼；片层结构；力学性能；强化机理

(Edited by Xiang-qun LI)